Hindawi
Advances in Civil Engineering
Volume 2024, Article ID 1951668, 14 pages
https://doi.org/10.1155/2024/1951668

Research Article

Water Sensitivity and Structural Properties of Loess

Longfei Zhang[1,2] **Zaiqiang Hu**[2] **Hongru Li**[2] **Haicheng She**[3] **Xiaoliang Wang**[2] **Xi Yang**[2] **and Xiaoning Han**[2]

[1]*School of Architectural Engineering, HuangHuai University, Zhumadian 463000, China*
[2]*Institute of Geotechnical Engineering, Xi'an University of Technology, Xi'an 710048, China,*
[3]*School of Urban Construction, Yangtze University, Jingzhou 434032, China*

Correspondence should be addressed to Zaiqiang Hu; huzq@xaut.edu.cn

Received 11 April 2023; Revised 24 November 2023; Accepted 3 May 2024; Published 15 May 2024

Academic Editor: Domenico Magisano

Loess has unique water sensitivity due to its distinct formation environment. The structure of loess is undercompactness, weak cementation, and porousness. The water sensitivity of loess directly leads to many environmental problems and geological hazards, including subgrade subsidences, slope collapse or failures, and building cracking. To reveal the relationship between water sensitivity and loess structure, confined-compression collapsibility tests and triaxial-collapsibility tests were performed on loess in different areas. The collapsibility coefficient, porosity ratio, and collapsibility rate were analyzed. Results show that the collapsibility process of loess can be divided into three stages: wetting, softening, and settling. The collapsibility sensitivity of loess is determined primarily by its structural and hydraulic state.

1. Introduction

Loess is a Quaternary sediment primarily formed by wind deposition. It accounts for more than 2.5% of the global land area and lacks distinct layering. Loess is rich in carbonate and contains numerous pores [1]. Due to variations in geology and climate in different regions, loess exhibits wide-ranging internal material compositions and external morphological characteristics. In its natural state, loess has high strength, large pores, and strong water absorption capacity. However, when a large amount of water infiltrates into loess, it destroys the interparticle cementation structure, leading to a rapid decrease in its bearing capacity [2]. This phenomenon is one of the main reasons for frequent engineering and natural disasters in loess regions. For example, the 2019 landslide in Zaoling Village, Yongning County, Shanxi Province, resulted in severe casualties and building damage [3]. In 2011, the Bailuyuan landslide in Baqiao District, Xi'an City, Shaanxi Province, caused 32 deaths. Landslides in the Heifangtai agricultural irrigation area in Gansu Province have also occurred multiple times, resulting in serious casualties [4, 5].

The sensitivity of loess to collapse refers to its characteristic of having high strength and low compressibility under natural moisture conditions but experiencing rapidly decreased strength and significantly increased deformation when subjected to inundation [6]. Due to the direct and evident impact of loess collapse sensitivity on engineering construction, researchers have focused on this topic for a long time and have achieved in-depth understanding [7–9]. Various explanations have been proposed for the mechanisms of loess collapse sensitivity, including the soluble-salt hypothesis [10], colloid-deficiency theory [11, 12], capillary hypothesis [13], underconsolidation theory [14], and structural theory [15–17].

The collapse sensitivity of loess is closely related to its skeletal structure and internal components, which are influenced by its formation process. Loess comprises mineral particles that have been transported by wind, sorted in the atmosphere, and deposited, resulting in a chaotic accumulation without distinct layering [18–20]. Coarse particles support one another, whereas fine particles adhere onto the surface of larger particles, forming a loess structure dominated by large pores with embedded micropores. When the soil layer accumulates to a certain thickness, short-term rainfall infiltrates the soil layer, gradually evaporating the water and reducing the moisture content. Consequently, the capillary water menisci at the contact points between particles

recede. A small amount of cementitious material, water, and dissolved salt ions remain, forming a certain level of interparticle bonding strength. When a new soil layer deposits onto the top of the existing layer, the pressure on the original layer increases. When the pressure between soil particles exceeds the bonding strength, the interparticle bonding is disrupted, and the soil structure transitions into a more stable state. Rainfall infiltration and evaporation accelerate this transition, forming new and stronger bonding, as well as the long-term natural conditions for the development of loess structure [21]. The external factors influencing loess collapse sensitivity are changes in stress and moisture conditions, the dissolution of soluble salts in loess, the deterioration of cementation, and microscopic structural damage, which ultimately affect the macroscopic strength and deformation behavior of loess.

Among many studies on loess collapse sensitivity, the structural theory attracts significant research attention. With advancements in observational techniques, the characteristics of loess collapse are being increasingly explained from a structural perspective, gaining widespread recognition [22, 23]. Loess structure encompasses the size, shape, surface characteristics, and spatial arrangement of constituent particles [24, 25] and the bonding form between skeletal particles and cementitious materials [26, 27], as well as the size, morphology, and distribution of pores [28, 29]. The ability of the soil to maintain its original structural state without disruption is used to measure the strength of the loess structure. When the structural state is disrupted, mechanical properties undergo a sudden change [30, 31]. Some scholars have approached the topic from the perspective of particle thermodynamics, establishing a thermal–water–force coupling mechanism for the particle rearrangement of saturated/unsaturated soils to consider the influence of stress paths and soil structure [32, 33]. However, relatively few systematic studies have been conducted on the "water sensitivity" of loess. Although some researchers have proposed the concept of "loess water sensitivity," they are still primarily focused on certain deformation behaviors of loess. Thus, gaining a deeper understanding of the mechanism of loess collapse and establishing a quantitative relationship between the microstructural elements of loess collapse sensitivity and its macroscopic behavior are essential [34, 35]. The topic has also been approached from the perspective of unsaturated soil mechanics, defining the mechanical process of loess water sensitivity as the compression and shear of the loess structure during the transition from unsaturated to saturated states. They believe that changes in matric suction are the primary cause of loess water sensitivity. Loess, as a typical unsaturated soil, is characterized by the soil–water characteristic curve, thereby effectively expressing the characteristics of unsaturated soil. Accordingly, studying the mechanical mechanism of loess water sensitivity from the perspective of unsaturated soil mechanics can effectively unify various phenomena related to loess water sensitivity [36]. However, traditional matric suction does not fall within the stress domain, so effectively establishing a bridge between "water" and "force" is challenging. Furthermore, matric suction covers a wide range of numerical values, conferring difficulty in providing a unified description for various mechanical behaviors and thus hindering its application in engineering practice. Therefore, some scholars have skipped directly to matric suction and analyzed the lateral displacement characteristics of soil and single piles under cyclic loading. The influences of groundwater level and cyclic load magnitude on the performance of the pile–soil system are examined [37, 38]. In summary, further exploration is needed to effectively describe the mechanism of loess water sensitivity.

The present study analyzes the entire process of loess, from its natural state to nonsaturated wetting-induced collapse and saturated collapse, by incorporating research on the structural nature of loess. The time factor is introduced to reflect the disturbance sensitivity of the loess structure's potential changes under compression and the water-wedge effect on potential changes under moisture infiltration. Some exploratory suggestions regarding the research on loess collapse sensitivity are also presented, thereby contributing to a beneficial attempt in advancing the study on loess.

2. Test Materials and Methods

To study the water sensitivity and structural characteristics of loess, laterally confined collapsibility tests and K_0 consolidation triaxial-collapsibility tests were conducted on undisturbed and remolded loess in the north side plot of Yangling and Xi'an, respectively.

2.1. Loess for Testing. The loess used in the test was collected from Yangling Arboretum and Jinghe New City and Xi'an Xixian new district. In the Yangling region, the soil was sampled at a depth of 5 m, classified as Q_3 Malan loess from the middle-late Pleistocene, dating back approximately 120,000 to 130,000 years. In the Xi'an region, the soil was sampled at a depth of 3 m, belonging to the Q_4 early Holocene Malan loess, dating back approximately 10,000 to 20,000 years. Its physical and mechanical parameters are shown in Table 1.

When preparing undisturbed loess samples, a circular soil cutter was used to shape the undisturbed loess into cylindrical specimens with dimensions of 39.1 mm × 40 mm and 39.1 mm × 80 mm, respectively. Subsequently, the samples were wrapped in cling film and stored in a humidification tank for subsequent testing applications. When preparing remolded loess samples, we start by air-drying the soil and sieving out particles larger than 2 mm. We measure its moisture content, calculate the required water mass based on the target moisture content, and spray the corresponding amount of water using a spray bottle. We allow the moistened soil to stand in a humidification tank for 2 days before sampling. Sample compaction is conducted in layers (each layer 2 cm thick) during the sampling process.

2.2. Microstructural Testing of Loess. This study conducted structural testing on two types of undisturbed loess using scanning electron microscope (SEM) imaging, focusing on the analysis of pore distribution and average diameter. The instruments used are shown in Figure 1, where Figure 1(a) represents the JFC-1600 ion sputtering instrument, capable of sputtering conductive films onto nonconductive loess samples. The resulting coating has fine, dense, uniform particles with strong adhesion. Figure 1(b) shows the JSM-6700F field emission scanning electron microscope, which enables microscopic morphological analysis, size analysis, material

Table 1: Basic physical parameters of tested loess.

Location of loess sample	Specific gravity of loess particles, G_s	Natural dry density, (ρ_d/g · cm^{-3})	Void ratio (e)	Water content, (ω %)	Plastic limit, (ω_p %)	Liquid limit, (ω_L %)	Plasticity index, I_p
Yangling	2.72	1.24	1.20	17.23	18.82	29.76	10.94
Xi'an	2.70	1.33	0.93	16.45	19.90	32.80	12.90

(a) (b)

Figure 1: Soil structural testing equipment: (a) JFC-1600 ion sputtering instrument and (b) JSM-6700F field emission scanning electron microscope.

microstructure, phase composition, and phase distribution analysis for various materials. Under low magnification conditions, the maximum magnification is 19,000x, and the resolution can reach 1 nm.

The classification of loess pores follows the standards outlined in [39], where micropores have diameters less than 2 μm, small pores have diameters of 2–8 μm, mesopores have diameters of 8–32 μm, and macropores have diameters greater than 32 μm. Prior to sample testing, it is necessary to dry and grind the samples, with specific methods outlined in [40, 41].

2.3. Collapsibility Test under Confined-Compression Conditions. The instrument used for the collapsibility test under confined-compression conditions was an FGJ-20 unsaturated soil consolidation instrument. To wet the loess samples in stages, we had to retrofit the instrument. The instrument was modified by setting a small water-inlet hole in the upper cap of the sample, which was connected to a double-layer organic glass tube that can control the pressure inside the tube. The inner tube had a diameter of 4 mm and was directly connected with the water inlet. The water inflow can be accurately measured, as shown in Figure 2. During the experiment, samples of undisturbed loess and remolded loess were subjected to different pressures under natural water-content conditions, and the samples were then wetted to saturation after deformation stabilized before applying the next level of the load. The relationship between the collapsible deformation of soil samples and time at each pressure level until the sample stabilized was determined. For the stability standard, the deformation per hour was less than 0.01 mm.

2.4. Collapsibility Test under K_0 Consolidation Conditions. The collapsibility test under the K_0 consolidation condition used a stress-controlled triaxial apparatus, as shown in Figure 3. An air compressor applied axial load and confining pressure during the test. First, the K_0 values of Yangling and Xi'an loess were obtained through conventional triaxial tests. After loading the sample, the confining and axial pressures were simultaneously applied to different pressures. In the K_0 consolidation triaxial immersion test, the Yangling soil samples were subjected to confining pressures σ_3 of 25.5, 51, and 102 kPa, whereas the Xi'an soil samples were subjected to confining pressures σ_3 of 30, 60, and 120 kPa. When the consolidation deformation was stable, we kept the stress state unchanged. The sample was immersed in water through the top of the triaxial sample, and the immersion device was operated through a calibrated drainage pipe. During the test, the immersion pipe was always in the open state, and water was replenished to the drainage pipe through a measuring cup to ensure that the sample was in a saturated state until the collapse deformation was stable. We determined the relationship among axial deformation, volume change, and time during the experiment until the sample was stable. For the stability standard, the deformation per hour was less than 0.01 mm.

The collapsibility coefficient is calculated according to Equation (1) [20]:

$$\delta_s = \frac{h_p - h_{p'}}{h_0}, \tag{1}$$

where h_p is the height of the loess sample when the deformation is stable under pressure P condition, $h_{p'}$ is the deformation of the loess sample when the deformation is stable under immersion condition, and h_0 is the original height of the loess sample.

2.5. Collapsibility Test under the Condition of Wetted in Stages and K_0 Consolidation Conditions. The instrument for the collapsibility test under wetting in stages and K_0

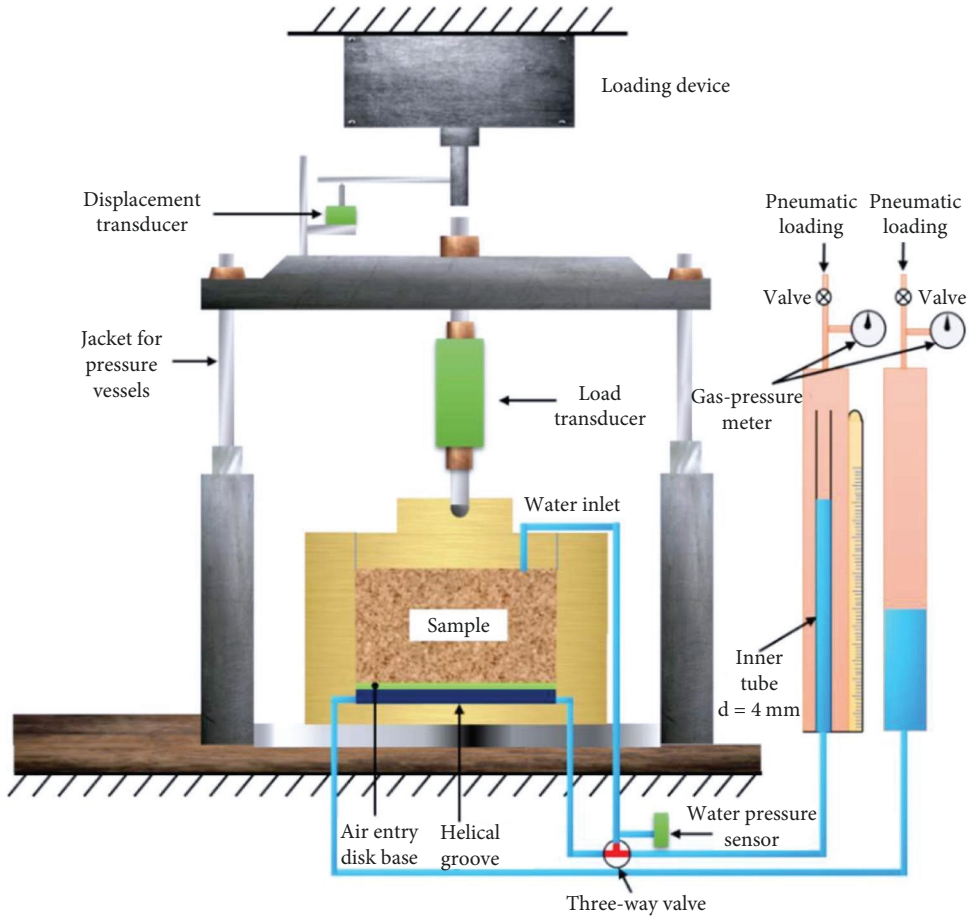

Figure 2: Instrument of collapsibility test under confined-compression condition.

consolidation condition was the same as that described in Section 2.3. The applied confining pressure was the same as that applied in the collapsibility test under the K_0 consolidation conditions. The Yangling soil samples were subjected to confining pressures σ_3 of 27.5, 55, and 110 kPa, whereas the Xi'an soil samples were subjected to confining pressures σ_3 of 30, 60, and 120 kPa. The difference was that we divided the immersion into three levels to complete. After each level of immersion, we waited for the deformation to stabilize before proceeding to the next level of immersion. The relationship among axial deformation, volume change, and time during the experiment until the sample stabilized was also determined. For the stability standard, the deformation per hour was less than 0.01 mm.

3. Results and Discussion

3.1. Microstructure of Two Types of Loess

3.1.1. Qualitative Analysis. The structural characteristics of loess are closely related to its contact with the skeleton, pore features, and bonding methods. Figure 4 shows the microstructure morphology of two types of loess magnified by 500x and 3,000x, respectively. In Figure 5(c), a magnified image within the red box of Figure 5(a) is presented, and in Figure 5(d), a magnified image within the red box of Figure 5(b) is shown. It can be observed that in the Yangling area, loess skeleton particles are mainly aggregated, and the pores are relatively well-developed. In the Xi'an area, there are numerous clump-shaped particles in the loess, with larger contact areas between particles, often exhibiting face-to-face contact, and relatively fewer pores.

3.1.2. Quantitative Analysis. To quantitatively analyze the microstructure of the two undisturbed loess samples, SEM images at a magnification of 500x were selected. After binarization processing (Figure 4), it was observed that the loess samples from the Yangling region had more and larger pores compared to those from the Xi'an region. Finally, pore classification and staining were applied for a clearer visualization of this pattern (Figure 6). Using IPP 6.0 software, we conducted a statistical analysis of the area ratios of four pore types (the proportion of each pore type area to the total pore area), and the results are presented in Table 2. It can be observed that in the Yangling region, micropores and mesopores dominate, with a small percentage of large pores, while in the Xi'an region, micropores and small pores are predominant, and large pores are absent.

3.2. Analysis of Collapsibility Test

3.2.1. Determination of K_0. Jaky's empirical equation was used to calculate K_0. Equation (2) shows the calculation method:

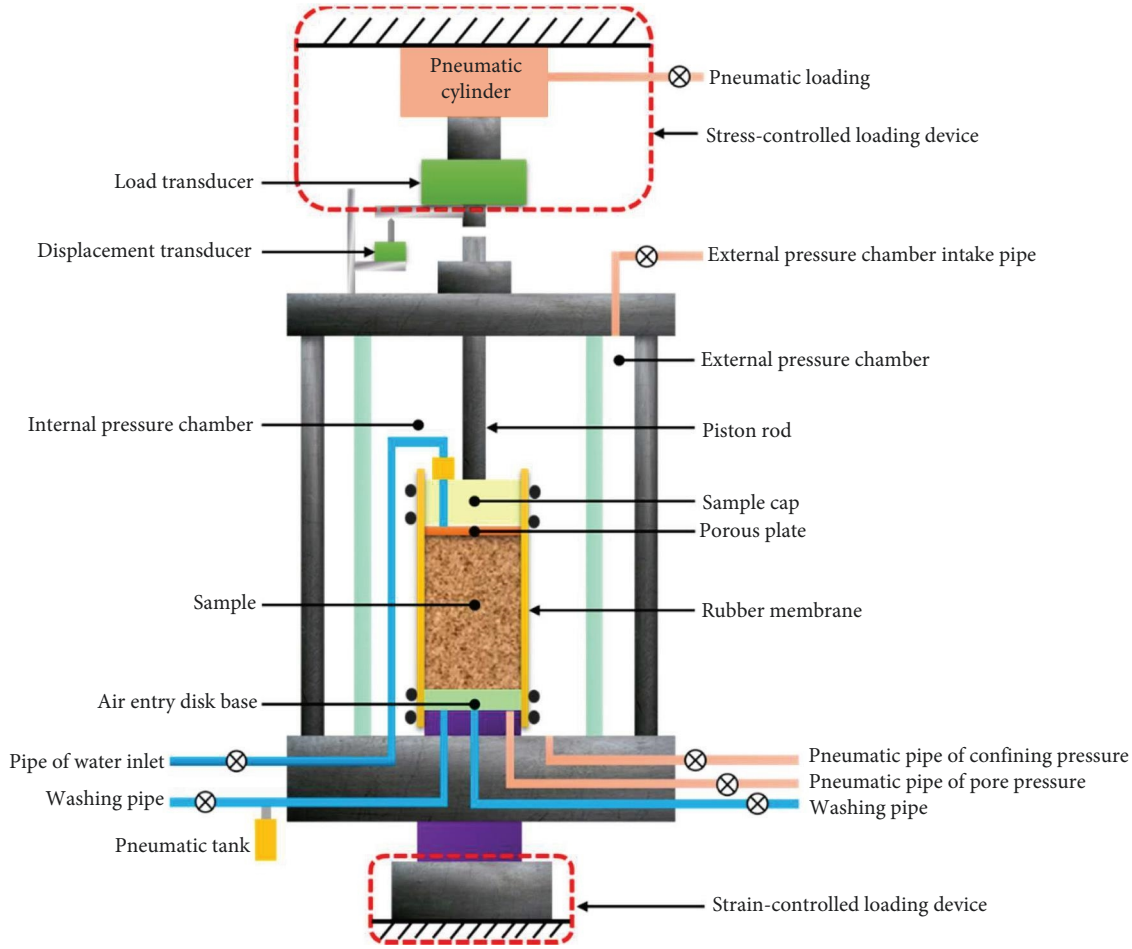

Figure 3: Instrument of collapsibility test under K_0 consolidation condition.

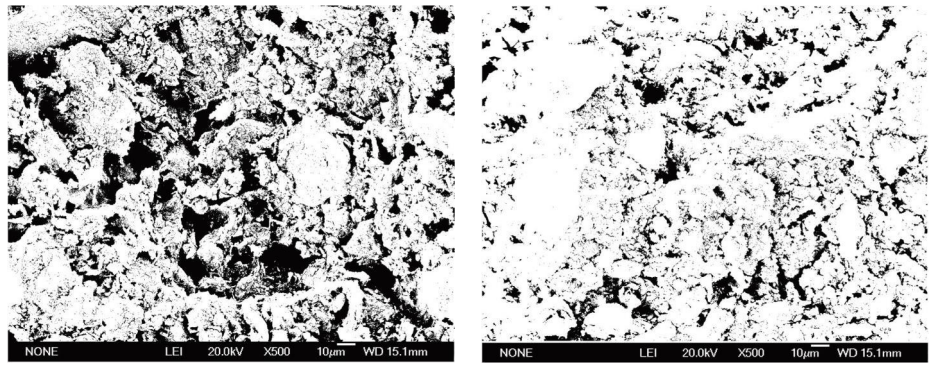

(a) (b)

Figure 4: Binary image: (a) Yangling and (b) Xi'an.

$$K_0 = 1 - \sin\varphi', \quad (2)$$

φ' is the effective internal friction angle determined through conventional triaxial tests. The experiment determined that $K_0 = 0.55$ in Yangling and $K_0 = 0.60$ in Xi'an.

3.2.2. Collapse Characteristics under Confined-Compression Condition. In Figure 7, illustrating the relationship curve between the amount of collapsible strain and immersion pressure, four distinct stages are identified based on deformation characteristics. The first stage represents additional compression deformation, demonstrating a linear change

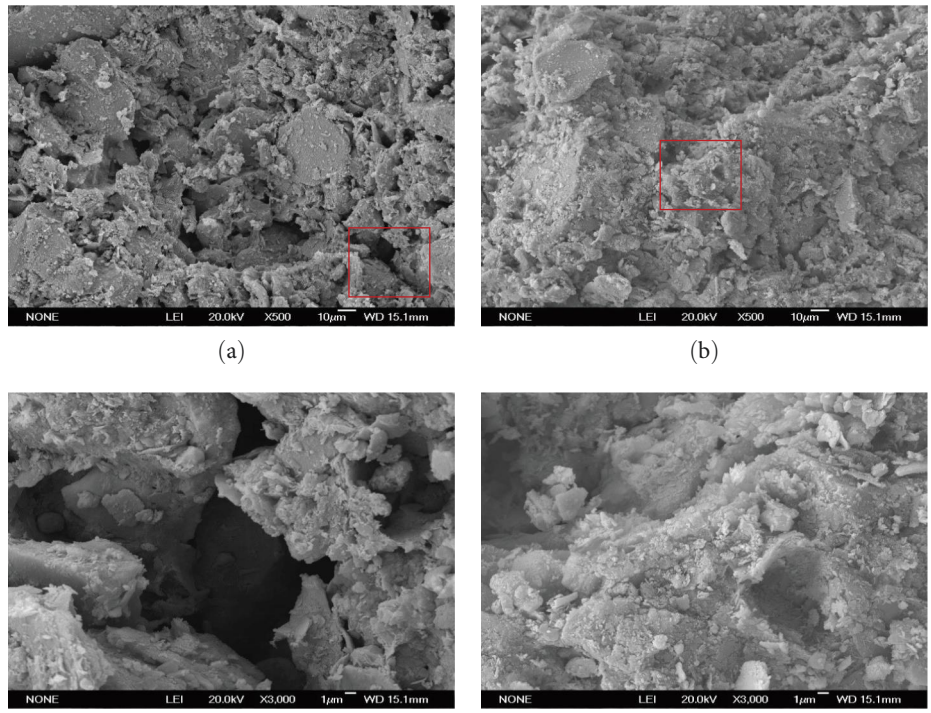

Figure 5: SEM scanned images: (a) 500x magnified photo of loess in Yangling, (b) 500x magnified photo of loess in Xi'an, (c) 3,000x magnified photo of loess in Yangling, and (d) 3,000x magnified photo of loess in Xi'an.

indicative of minimal structural damage. During this phase, the loess experiences a reduction in pore volume without compromising the arrangement structure between sample particles. The second stage marks the initiation of collapsible deformation, characterized by the disruption of connections between loess particles as external pressure surpasses the residual structural strength. Even a slight increase in pressure leads to significant deformation, reflected in the increasing slope of the curve. Moving to the third stage, the development of collapsible deformation is characterized by rapid and substantial deformations, reaching the maximum slope of the curve. This stage involves significant changes in the internal structure of the loess, with the disruption of particle connections and a notable shift in the arrangement of particles. The fourth stage, identified as the decline stage of collapsible deformation, indicates a decrease in the deformation amplitude and collapsibility. This decline is attributed to the constraint effect of the ring knife side wall, preventing lateral extrusion during collapsibility. Under external load, the compactness of the sample gradually increases, the pore ratio decreases, and the particle arrangement becomes more compact.

A higher dry density corresponds to a smaller pore ratio and reduced collapsible deformation caused by loess. It is worth noting that undisturbed loess formed under arid or semiarid climates possesses a certain structural strength. During the low-pressure wetting stage, it exhibits minimal compression deformation. Significant collapse deformation only occurs when the pressure surpasses a specific threshold, termed the initial collapse pressure. In contrast, remolded loess, having undergone a reshaping process where the original structure is disrupted, exhibits a more uniform particle arrangement. Its collapsible characteristics are more pronounced in experiments, showing significant collapse deformation even at lower pressures. Figure 7 also reveals that the initial collapse pressure of loess in the Xi'an area is smaller than that in the Yangling area.

3.2.3. Collapse Characteristics under K_0 Consolidation Condition. Figure 8 shows the relationship curve between the collapsible strain and pressure of loess after immersion in water under triaxial conditions. Due to the lack of lateral wall constraints, the loess sample experiences lateral extrusion, resulting in the continuous development of loess collapsibility until reaching the maximum deformation value under a certain pressure. Comparing the collapse deformation curves of the two regions, we can see that the original loess with low dry density, large pore ratio, and high water content in the Yangling area has a lower initial collapse pressure than that in the Xi'an area.

3.2.4. Collapse Characteristics under the Wetted Condition in Different Stages and K_0 Consolidation Condition. The K_0 consolidation state is the stress state of the foundation before immersion. With the development of the immersion process, the loess reaches the corresponding water content, and under a certain pressure, collapse occurs. With the increased immersion amount, deformation also increases. Figure 9 represents the relationship curve between collapsibility coefficient and water content specifically for the Xi'an region. The collapsible deformation of loess is not significant under low-stress levels. However, even with a small amount of water immersion at larger stress levels, collapsible deformation can reach 40%–60% of the total

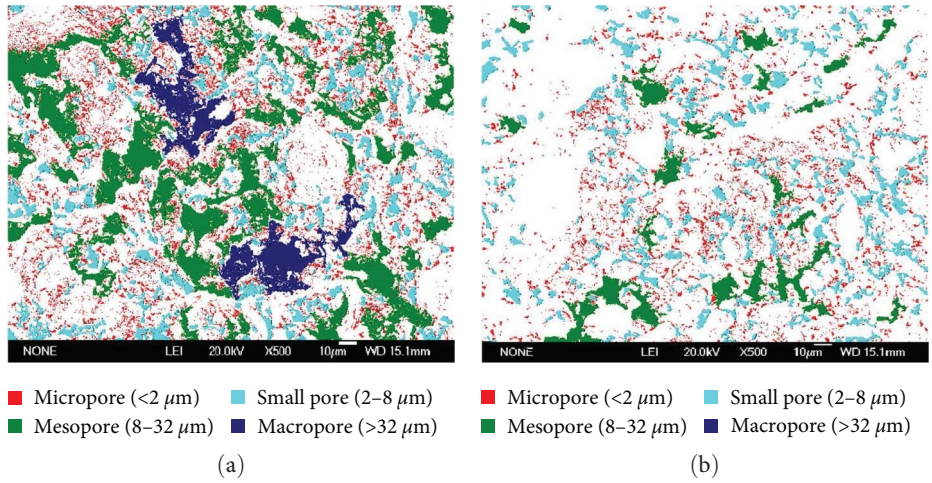

Figure 6: Pore distribution image classified by average pore diameter: (a) Yangling and (b) Xi'an.

Table 2: Area ratios of different pore sizes in loess samples.

Location of loess sample	Maximum diameter, (d_{mean} μm)	Area ratios, S			
		Micropore	Small pore	Mesopore	Macropore
Yangling	36.2	0.52	0.04	0.34	0.10
Xi'an	16.2	0.69	0.25	0.06	0

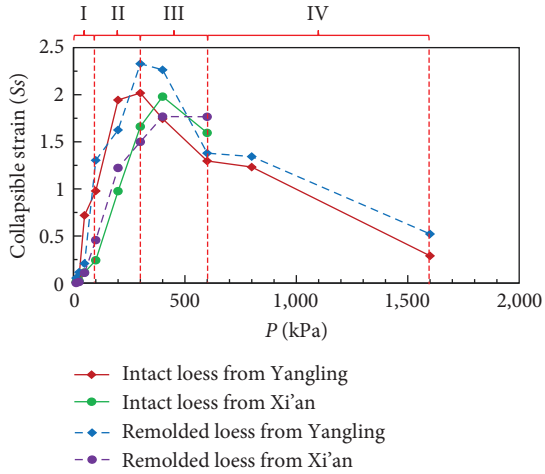

Figure 7: Relationship curve of collapse deformation vs. immersion pressure under confined compression conditions.

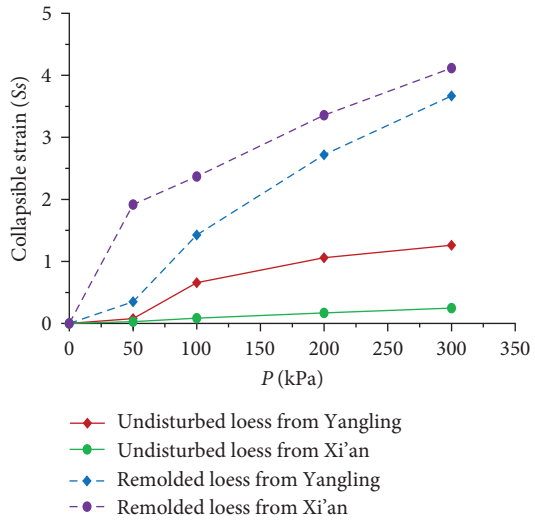

Figure 8: Relationship curve of collapse deformation vs. immersion pressure under K_0 consolidation conditions.

collapsible deformation. Thus, the harm of a small amount of wetting of collapsible loess to buildings cannot be ignored.

Figure 10 shows that under graded humidification conditions, the collapsibility coefficient of loess changes more slowly with time than under saturated conditions. The change in the pore ratio is not significant at each humidification stage, and the collapsibility deformation rate is exponentially correlated with time.

3.3. Relationship between Loess Collapse Deformation and Time. The process of loess collapsibility when encountering water is very rapid. What are the characteristics of the collapsibility rate over time during this period? This section analyzes the characteristics of compression deformation and collapse deformation of loess over time by K_0 consolidation compression tests and collapsibility tests on undisturbed and remolded samples.

Figures 11–13 show the variation curves of the collapsibility coefficient, collapse speed, and void ratio over time of undisturbed and remolded loess in the Yangling area under different confining pressures. In this study, the settlement rate "v" of loess is defined as the magnitude of change in

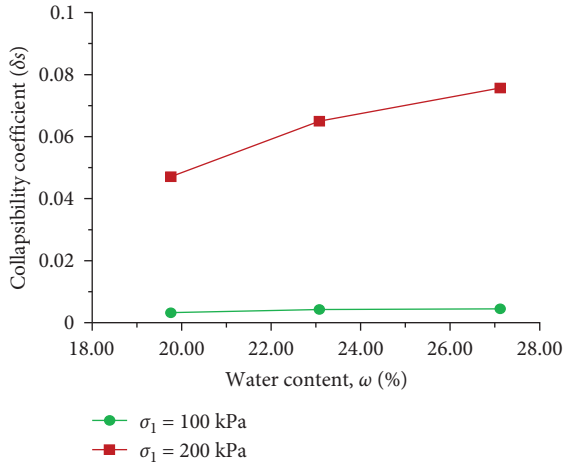

Figure 9: Relationship curve between collapsibility coefficient and water content.

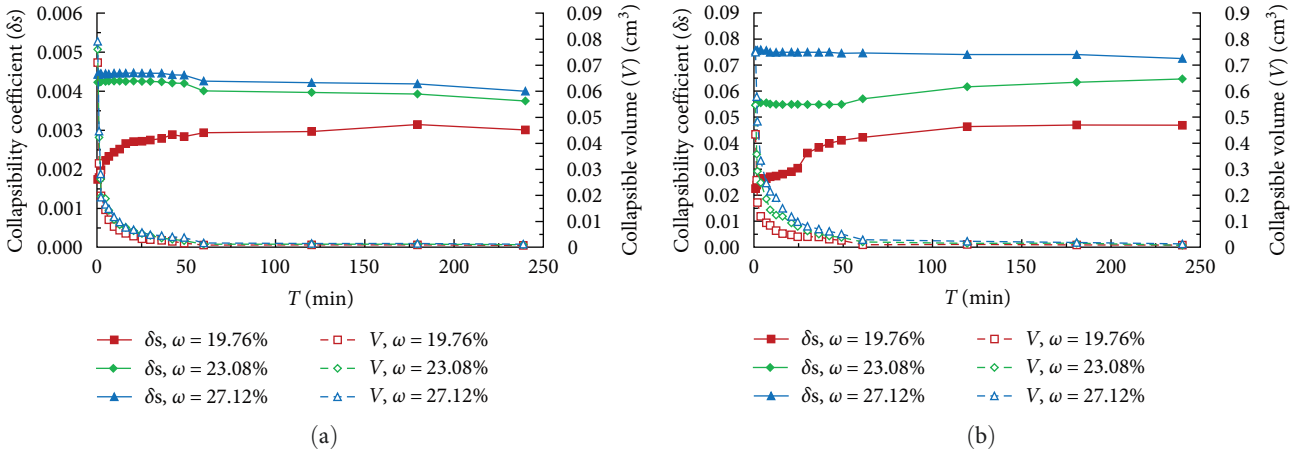

Figure 10: Time variation curve of collapse coefficient and collapse volume: (a) $\sigma_1 = 100$ kPa and (b) $\sigma_1 = 200$ kPa.

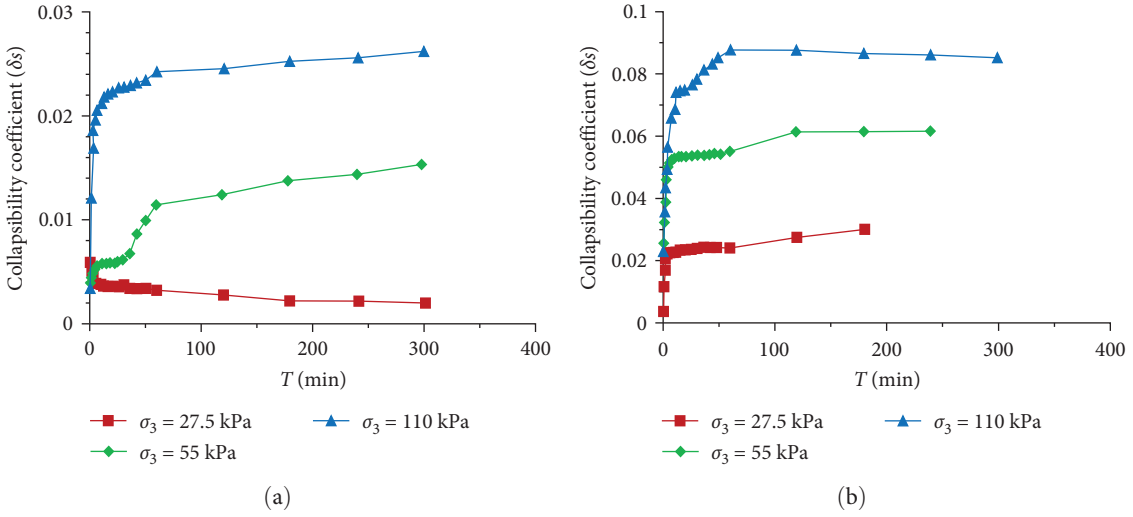

Figure 11: Curves of collapse coefficient with time in Yangling area: (a) undisturbed loess and (b) remolded loess.

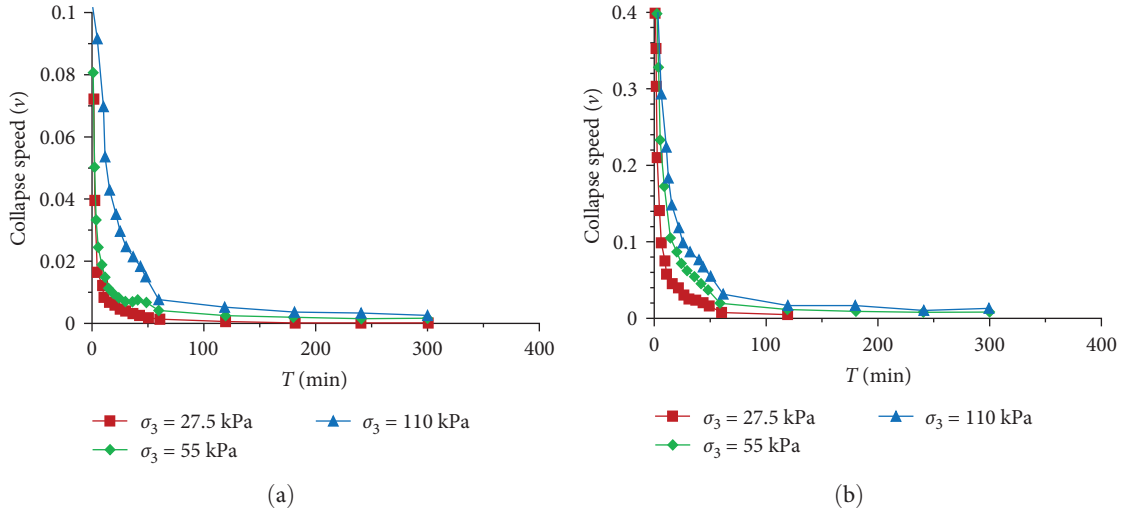

Figure 12: Curves of collapse speed with time in Yangling area: (a) undisturbed loess and (b) remolded loess.

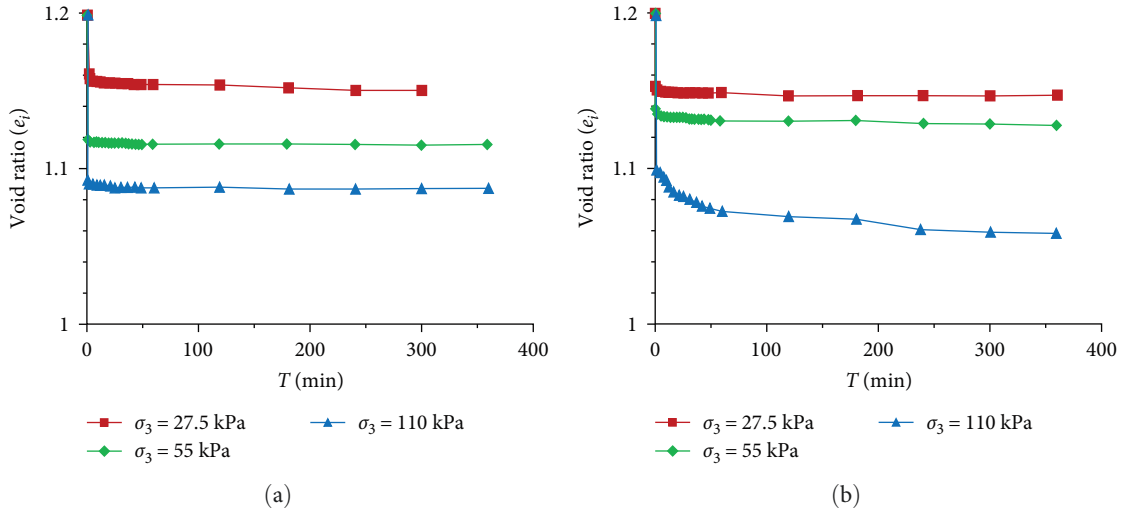

Figure 13: Curves of void ratio with time in Yangling area: (a) undisturbed loess and (b) remolded loess.

settlement over different time periods, which can be expressed by Equation (3). During the settlement process, the microstructure of the soil undergoes continuous changes, resulting in varying magnitudes of settlement at different time intervals. Therefore, the collapse speed of loess is a variable quantity, and the magnitude of the collapse speed signifies the development rate of loess settlement, known as settlement sensitivity. Different settlement sensitivities can cause varying degrees of damage to structures. Hence, quantitatively representing the collapse speed of loess holds practical significance.

$$v = \frac{h_n - h_{n-1}}{t_n - t_{n-1}}, \tag{3}$$

where h_n and h_{n-1} represent the corresponding values of soil settlement at specific time points; t_n and t_{n-1} represent the corresponding time points of measurement.

Similar to the confining-compression test results, the collapsible deformation of loess under slight pressure is not significant, and the collapsible deformation gradually increases with increased pressure. When $K_0 < 0.4$, the collapsibility coefficient measured using the triaxial method is generally more significant than the confining-compression test. Conversely, when $K_0 \geq 0.4$, the collapsibility coefficient measured using the triaxial method is generally smaller than the confining-compression test [42]. This experiment also proves this viewpoint. Figures 12 and 13 show that the collapse deformation of loess occurs suddenly after immersion. At the initial moment, the deformation is maximum, and as time increases, the deformation speed gradually decreases and finally stabilizes. The triaxial test data further confirm that once a building is subject to collapse, the initial stage is significantly affected and is closely correlated with the load on the loess.

Figures 14–16 show the curves of the collapsibility coefficient, collapse speed, and void ratio over time of undisturbed

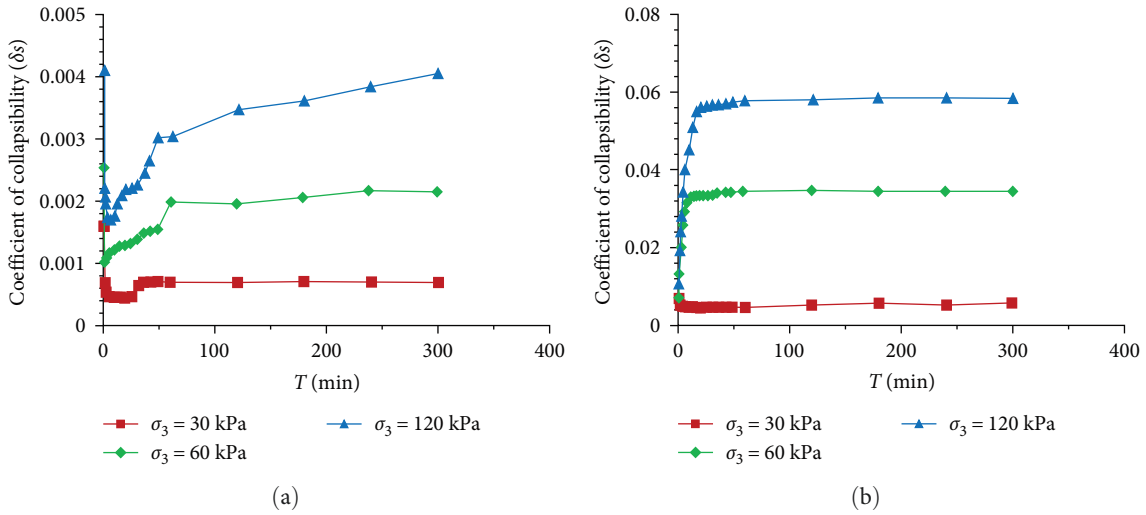

Figure 14: Curves of collapse coefficient with time in Xi'an area: (a) undisturbed loess and (b) remolded loess.

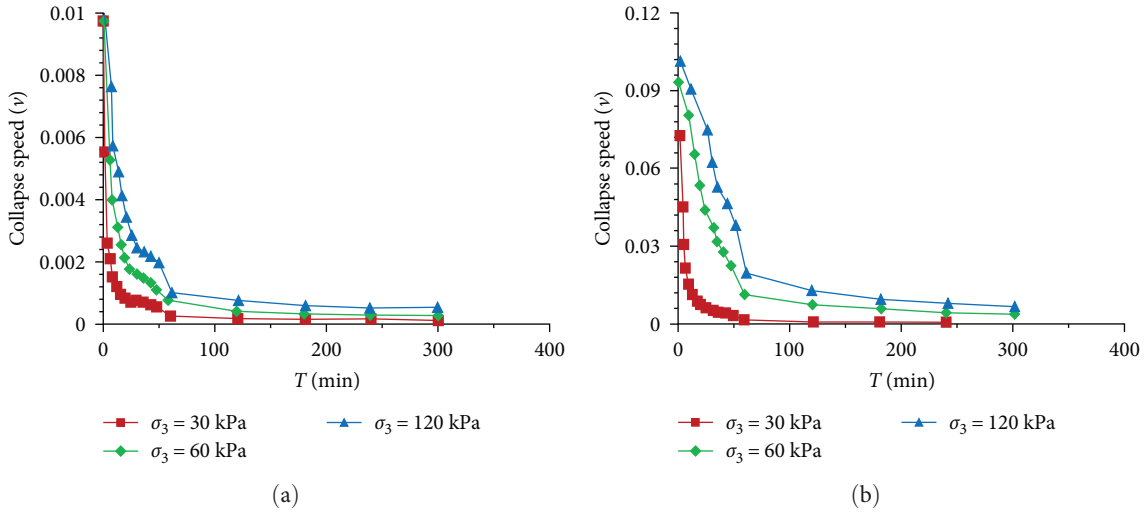

Figure 15: Curves of collapse speed with time in Xi'an area: (a) undisturbed loess and (b) remolded loess.

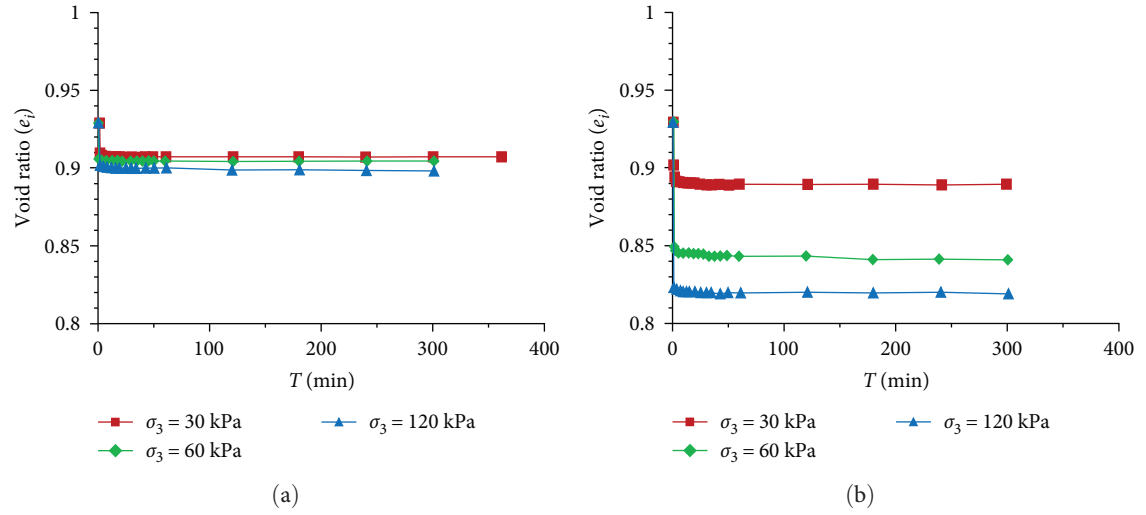

Figure 16: Curves of void ratio with time in Xi'an area: (a) undisturbed loess and (b) remolded loess.

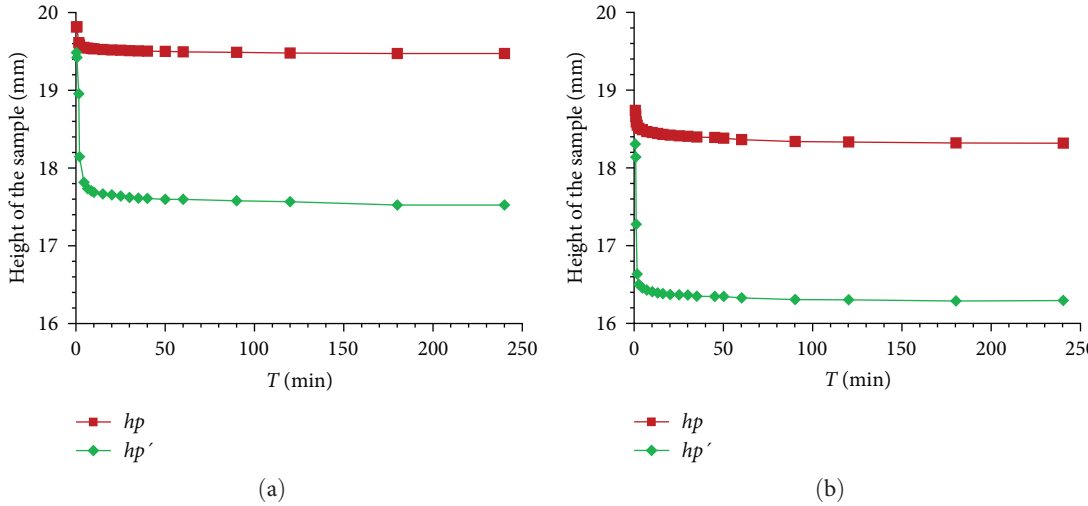

Figure 17: Changes in sample height over time under different pressures P: (a) $P = 200$ kPa and (b) $P = 300$ kPa.

and remolded loess in the Xi'an area under different confining pressures. Comparison reveals that the collapsibility of undisturbed loess in the Xi'an area is significantly weaker than that in the Yangling area. From the overall trend, loess with low dry density, large pore ratio, and high water content is found to have an early onset of collapse pressure and peak collapse and is more prone to collapse under low pressure.

Collapse deformation belongs to plastic deformation generated under the combined action of force and water. The action of water induces changes in the physical state and structural strength of loess, which is a necessary condition for the occurrence of collapse. The role of force is the dominant factor destroying the loess structure, which can lead to plastic deformation. The amount of immersion and stress state also determines the degree of plastic flow. A specific combination of stress and moisture content corresponds with a certain amount of collapsible deformation, and the continuous changes in stress and moisture content correspond with a series of continuous changes in collapsible plastic deformation. For specific collapsible loess (the initial density, water content, and void ratio of loess have been determined), and its constitutive equation can be written as Equation (4):

$$\boldsymbol{\varepsilon}_{ij}^{ab} = f\left(\boldsymbol{\sigma}_{ij}, w, t\right), \tag{4}$$

where $\boldsymbol{\varepsilon}_{ij}^{ab}$ is the deformation tensor of collapse, $\boldsymbol{\sigma}_{ij}$ is the stress tensor, and w is the water content at time t.

In previous studies, only the deformation of loess at the beginning and after stabilization of collapse has been considered, so it cannot reflect the changes in the rate during collapse. Accordingly, the author believes that studying the continuous changes in the rate of collapse during collapse, particularly the changes in a short time, is necessary. Due to the change in height and pore ratio, the main reason for loess collapse is due to its height and pore ratio. The pore ratio varies depending on the pressure and water content. Thus, as long as these two items are clear, we can determine the collapse coefficient at any time. Therefore, if we compare the continuous collapse coefficient obtained, we can calculate the collapsibility rate at a specific water content and pressure. As mentioned above, establishing an indicator that ignores other factors and considers only the temporal influence of collapsible deformation over time is possible.

Figure 17 shows the variations in sample height over time for undisturbed loess in the Xi'an region under different pressures P. The graph reveals a discernible pattern in the relationship between various pressure levels P in both scenarios (h_p and h_p'), which can be fitted as Equations (5) and (6):

$$h_p = B_1 \cdot e^{\alpha t} + B_2 \cdot e^{\beta t} + y_0, \tag{5}$$

$$h_p^{'} = B_3 \cdot e^{\gamma t} + B_4 \cdot e^{\eta t} + y_{0'}. \tag{6}$$

Therefore, the time-influencing factor indicator proposed in this article can be expressed as follows:

$$\delta_s = \frac{h_p - h_p^{'}}{h_0} = \frac{{}_1 \cdot e^{\alpha t} + B_2 \cdot e^{\beta t} + y_0 - B_3 \cdot e^{\gamma t} - B_4 \cdot e^{\eta t} - y_{0'}}{h_0}. \tag{7}$$

To verify the rationality of this indicator, this article compared the experimental data with the calculated values, and the results are shown in Figure 18. The calculated values well agree with the experimental one, confirming that the time-influencing factor index proposed in this article is reliable. This indicator reflects the process of the changes in the collapsibility coefficient over time and can also reflect the changes in the collapsibility rate during the collapsibility process.

3.4. Collapsibility Coefficient of Volume. The collapse of loess generally occurs under the influence of force and water. Under a certain pressure, the collapsibility is very strong; if

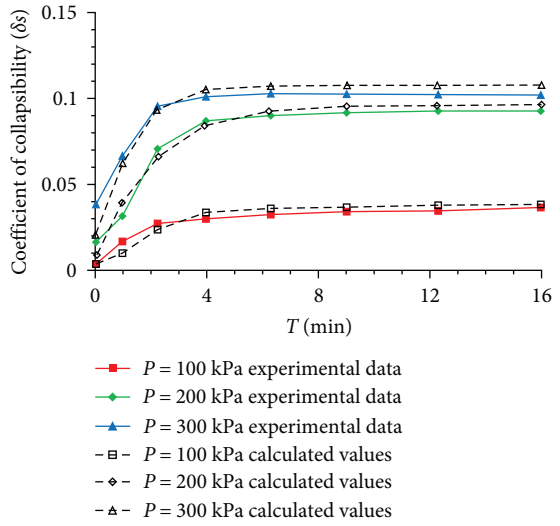

Figure 18: Comparison chart of calculated values and measurement values.

Table 3: Comparison between δ_s and δ_v.

Vertical load (kPa)	Undisturbed loess in Yangling area		Remolded loess in Yangling area		Undisturbed loess in Xi'an area		Remolded loess in Xi'an area	
	δ_s	δ_v	δ_s	δ_v	δ_s	δ_v	δ_s	δ_v
50	0.0007	0.0009	0.0091	0.0092	0.0021	0.0021	0.0487	0.0482
100	0.0023	0.0030	0.0358	0.0362	0.0166	0.0171	0.0614	0.0621
200	0.0042	0.0033	0.0544	0.0546	0.0266	0.0268	0.0839	0.0841

it is greater than or less than that pressure, the collapsibility weakens. Watering-induced collapse is a gradual process in which the loess becomes partially saturated quickly from the beginning of immersion. With the continuous infiltration of water, the collapse continues until the entire loess is saturated. The amount of water entering the loess varies under different pressures. When the pressure is high, the loess becomes compacted, and the amount of water immersed in the loess decreases. This finding also indicates that the collapsibility is not significant when the pressure is high. It is an essential indicator for determining loess collapsibility, type, and grade. The measurement of their collapsibility coefficient encompasses engineering treatment measures and associated costs, both of which are crucial considerations. We have accumulated considerable experience in measuring and using it as a standard for evaluating the collapsibility of loess. However, this coefficient is extremely unstable, and the calculated collapsibility is inconsistent with the actual situation. Therefore, there are two reasons for people's suspicion of this important collapsibility index:

(1) The collapsibility test was conducted using a compression apparatus, and the sample volume used was relatively small, which was greatly affected by the instrument boundary. For example, in the early stage of loading, the collapsibility coefficient is relatively high due to insufficient surface flatness of the loess sample and insufficient contact between the permeable stone and the surrounding wall of the instrument. In the later stage of compression, the loess sample undergoes a strengthening phenomenon due to the limitations of the instrument side wall.

(2) The measured values of the collapsibility coefficient are unstable and significantly influenced by instrument performance, operating techniques, and the degree of loess sample disturbance.

The impact of instrument performance, operational techniques, and loess sample disturbance cannot be avoided with the current testing methods and techniques. Thus, many scholars suggest using triaxial tests to determine the collapsible deformation law of loess. Based on the analysis of experimental data in this article, an equation for calculating the collapsibility coefficient under triaxial conditions called the volumetric collapsibility coefficient is proposed:

$$\delta_v = \frac{v_p - v'_p}{v_0}, \tag{8}$$

where δ_v is the coefficient of volumetric collapse, v_p is the volume of the loess sample when the deformation is stable under pressure P, v'_p is the volume of the above loess sample

when the deformation is stable after immersion in water, and v_0 is the initial volume of the loess sample.

The data in Table 3 show that the value calculated using δv is slightly larger than that calculated using δs. The data collected from the experiment reveal that the results in this interval remain satisfactory. Therefore, the volume collapse coefficient proposed in this article is reasonable.

4. Conclusions

(1) The loess structure is closely correlated with its collapse deformation, and the collapse process of loess is the gradual evolution of its structure under the action of water and force. A stronger structure of loess corresponds with a greater initial pressure of collapse and a greater rate of collapse after collapse initiation, and vice versa.

(2) Certain limitations exist in using the lateral limited collapsibility test to study the collapsibility characteristics of loess. Its collapsibility rate is relatively lower than that found in the triaxial-collapsibility test. The proposed method of measuring the volumetric collapsibility coefficient through the triaxial test can effectively compensate for the shortcomings of limited lateral collapsibility.

(3) The results of the triaxial immersion test indicate that loess also undergoes collapsible deformation when slightly immersed. The loess collapsibility coefficient's change rate with time under wetted-stage conditions is slower than that under saturated conditions. The change in the void ratio is not significant at each immersion stage, and the collapsible deformation rate remains exponential with time. However, the change is minor compared with that under saturation conditions.

Data Availability

The data used to support the findings of this study are included in the article.

Conflicts of Interest

The authors declare that they have no conflicts of interest regarding the publication of this article.

Authors' Contributions

Zhang Longfei proposed ideas and performed experiments. Li Hongru and She Haicheng designed the content, method, and technical route of the test and combined it with the actual situation to determine the test scheme. Wang Xiaoliang, Han Xiaoning, and Yang Xi provided assistance with materials and background knowledge. Hu Zaiqiang reviewed and edited the manuscript. All authors have read and agreed to the published version of the manuscript.

Acknowledgments

This work was supported by the Science and Technology Innovation Project of Key Laboratory of Shaanxi Province China (No. 2014SZS15–Z02), which is gratefully acknowledged.

References

[1] Y. Li, W. Shi, A. Aydin, M. A. Beroya-Eitner, and G. Gao, "Loess genesis and worldwide distribution," *Earth-Science Reviews*, vol. 201, Article ID 102947, 2020.

[2] X. Zhu, J. Gray, Y. Gu, and T. He, "Genesis of Loess Particles on the Chinese Loess Plateau," *Geochemistry, Geophysics, Geosystems*, vol. 23, no. 7, 2022.

[3] W. Shi, Y. Li, W. Zhang et al., "The loess landslide on 15 march 2019 in Shanxi Province, China," *Landslides*, vol. 17, no. 3, pp. 677–686, 2020.

[4] Q. Xu, W.-L. Li, Y.-Z. Ju, X.-J. Dong, and D.-L. Peng, "Multitemporal UAV-based photogrammetry for landslide detection and monitoring in a large area: a case study in the Heifangtai terrace in the Loess Plateau of China," *Journal of Mountain Science*, vol. 17, no. 8, pp. 1826–1839, 2020.

[5] Y.-J. Xu, J.-D. Wang, T.-F. Gu, and J.-X. Kong, "Geological hazards in loess induced by agricultural irrigation in arid and semiarid regions of China," *Advances in Civil Engineering*, vol. 2020, Article ID 8859166, 11 pages, 2020.

[6] G. B. Cazacu and G. Draghici, *The Geotechnical Properties, on Water Sensitive Soils, Loess*, Springer International Publishing, 2019.

[7] W. Zhang, N. Fan, Y. Li, S. He, and D. Guo, "Water-induced disintegration behaviour of Malan loess," *Earth Surface Processes and Landforms*, vol. 47, no. 8, pp. 1891–1901, 2022.

[8] H. Sadeghi, M. Kiani, M. Sadeghi, and F. Jafarzadeh, "Geotechnical characterization and collapsibility of a natural dispersive loess," *Engineering Geology*, vol. 250, pp. 89–100, 2019.

[9] J.-J. Nan, J.-B. Peng, F.-J. Zhu, J.-Y. Zhao, and Y.-Q. Leng, "Multiscale characteristics of the wetting deformation of Malan loess in the Yan'an area, China," *Journal of Mountain Science*, vol. 18, no. 4, pp. 1112–1130, 2021.

[10] K. Liu, T. Gu, X. Wang, and J. Wang, "Time-dependence of the mechanical behavior of loess after dry-wet cycles," *Applied Sciences*, vol. 12, no. 3, Article ID 1212, 2022.

[11] W. Ye, Y. Bai, C. Cui, and X. Duan, "Deterioration of the internal structure of loess under dry-wet cycles," *Advances in Civil Engineering*, vol. 2020, Article ID 8881423, 17 pages, 2020.

[12] L. Zuo, L. Xu, B. A. Baudet, C. Gao, and C. Huang, "The structure degradation of a silty loess induced by long-term water seepage," *Engineering Geology*, vol. 272, Article ID 105634, 2020.

[13] J. Xu, Y. Li, C. Ren, and W. Lan, "Damage of saline intact loess after dry-wet and its interpretation based on SEM and NMR," *Soils and Foundations*, vol. 60, no. 4, pp. 911–928, 2020.

[14] H. Yang, W.-L. Xie, Q.-Q. Liu, R.-S. Zhu, and Y.-Y. Liu, "Three-stage collapsibility evolution of Malan loess in the Loess Plateau," *CATENA*, vol. 217, Article ID 106482, 2022.

[15] L. Pan, J.-G. Zhu, and Y.-F. Zhang, "Evaluation of structural strength and parameters of collapsible loess," *International Journal of Geomechanics*, vol. 21, no. 6, pp. 1–12, 2021.

[16] Y.-Z. Hao, T.-H. Wang, and J.-J. Wang, "Structural properties of unsaturated compacted loess for various sample moisture contents," *Arabian Journal of Geosciences*, vol. 12, no. 8, pp. 1–10, 2019.

[17] Y. Qin, G. Li, X. Chen, and K. Fan, "Study on shear strength and structure of Malan loess under wetting–drying cycles," *Arabian Journal of Geosciences*, vol. 14, no. 24, pp. 1–12, 2021.

[18] L. Feng, M. Zhang, Z. Jin et al., "The genesis, development, and evolution of original vertical joints in loess," *Earth-Science Reviews*, vol. 214, Article ID 103526, 2021.

[19] Z. Zheng, X.-A. Li, and L. Wang, "A longitudinal analysis of collapsibility with predictions over the southeastern Loess Plateau in China," *Scientific Reports*, vol. 11, no. 1, pp. 1–17, 2021.

[20] Y. Leng, J. Peng, S. Wang, and F. Lu, "Development of water sensitivity index of loess from its mechanical properties," *Engineering Geology*, vol. 280, no. 2020, Article ID 105918, 2021.

[21] H. Chen, Y. Jiang, Y. Gao, and X. Yuan, "Structural characteristics and its influencing factors of typical loess," *Bulletin of Engineering Geology and the Environment*, vol. 78, no. 7, pp. 4893–4905, 2019.

[22] F. Ma, J. Yang, and X. Bai, "Water sensitivity and microstructure of compacted loess," *Transportation Geotechnics*, vol. 11, pp. 41–56, 2017.

[23] X. Zhang, Y. Lu, X. Li, Y. Lu, and W. Pan, "Microscopic structure changes of Malan loess after humidification in South Jingyang Plateau, China," *Environmental Earth Sciences*, vol. 78, no. 10, pp. 1–12, 2019.

[24] X.-A. Li, L. Li, Y. Song, B. Hong, L. Wang, and J. Sun, "Characterization of the mechanisms underlying loess collapsibility for land-creation project in Shaanxi Province, China—a Study from a micro perspective," *Engineering Geology*, vol. 249, pp. 77–88, 2019.

[25] T. Jian, L. Kong, W. Bai, and Z. Sun, "Investigation on compressibility and microstructure evolution of intact loess at different wetting States," *Frontiers in Earth Science*, vol. 10, pp. 1–13, 2022.

[26] Y.-Z. Wei, Z.-H. Yao, X.-L. Chong, J.-H. Zhang, and J. Zhang, "Microstructure of unsaturated loess and its influence on strength characteristics," *Scientific Reports*, vol. 12, no. 1, pp. 1–20, 2022.

[27] P. Li, S. Shao, T. Xiao, and D. Zhu, "Pore-size distribution evolution of intact, compacted, and saturated loess from china during consolidation and shearing," *Advances in Civil Engineering*, vol. 2021, Article ID 6644471, 14 pages, 2021.

[28] T. P. Mokritskaya, A. V. Tushev, K. A. Samoylich, and P. N. Baranov, "Deformations of loess soils caused by changes in the microaggregate structure," *Bulletin of Engineering Geology and the Environment*, vol. 78, no. 5, pp. 3729–3739, 2019.

[29] M. Zhao, H.-G. Wu, W. Guo et al., "Experimental study of the particle agglomeration on its mechanical properties of collapsible loess," *Frontiers in Earth Science*, vol. 10, pp. 1–13, 2022.

[30] P. Li, Z. Pan, T. Xiao, and J. Wang, "Effects of molding water content and compaction degree on the microstructure and permeability of compacted loess," *Acta Geotechnica*, vol. 18, no. 2, pp. 921–936, 2023.

[31] X.-A. Li, J. Sun, H. Ren, T. Lu, Y. Ren, and T. Pang, "The effect of particle size distribution and shape on the microscopic behaviour of loess via the DEM," *Environmental Earth Sciences*, vol. 81, no. 10, pp. 1–17, 2022.

[32] B. Bai, R. Zhou, G. Cai, W. Hu, and G. Yang, "Coupled thermo-hydro-mechanical mechanism in view of the soil particle rearrangement of granular thermodynamics," *Computers and Geotechnics*, vol. 137, Article ID 104272, 2021.

[33] B. Bai, S. Jiang, L. Liu, X. Li, and H. Wu, "The transport of silica powders and lead ions under unsteady flow and variable injection concentrations," *Powder Technology*, vol. 387, pp. 22–30, 2021.

[34] Z. Zheng, X. an Li, L. Wang, L. Li, J. Shi, and M. Bi, "A new approach to evaluation of loess collapsibility based on quantitative analyses of colloid-clay coating with statistical methods," *Engineering Geology*, vol. 288, Article ID 106167, 2021.

[35] J.-D. Wang, P. Li, Y. Ma, S. K. Vanapalli, and X.-G. Wang, "Change in pore-size distribution of collapsible loess due to loading and inundating," *Acta Geotechnica*, vol. 15, no. 5, pp. 1081–1094, 2020.

[36] Q. Li, T. Li, W. Shen et al., "Significance of the van der Waals force on the formation of the microstructure of wind-blown loess: an investigation using modified discontinuous deformation analysis," *Computers and Geotechnics*, vol. 148, Article ID 104833, 2022.

[37] B. Yuan, Z. Li, W. Chen et al., "Influence of groundwater depth on pile-soil mechanical properties and fractal characteristics under cyclic loading," *Fractal and Fractional*, vol. 6, no. 4, Article ID 198, 2022.

[38] B. Yuan, M. Chen, W. Chen, Q. Luo, and H. Li, "Effect of pile-soil relative stiffness on deformation characteristics of the laterally loaded pile," *Advances in Materials Science and Engineering*, vol. 2022, Article ID 4913887, 13 pages, 2022.

[39] P. Xu, Q. Zhang, H. Qian, W. Qu, and M. Li, "Microstructure and permeability evolution of remolded loess with different dry densities under saturated seepage," *Engineering Geology*, vol. 282, no. 2020, Article ID 105875, 2021.

[40] P. Xu, Q. Zhang, H. Qian, M. Li, and F. Yang, "An investigation into the relationship between saturated permeability and microstructure of remolded loess: a case study from Chinese loess plateau," *Geoderma*, vol. 382, no. 2020, Article ID 114774, 2021.

[41] P. Xu, H. Qian, Q. Zhang, J. Shang, Y. Guo, and M. Li, "Response mechanism of permeability change of remolded loess to seepage parameters," *Journal of Hydrology*, vol. 612, Article ID 128224, 2022.

[42] Z. Li, X. Li, Y. Zhu, S. Dong, C. Hu, and J. Fan, "Mining and analysis of multiple association rules between the Xining loess collapsibility and physical parameters," *Scientific Reports*, vol. 11, no. 1, pp. 1–13, 2021.